WPS1-PR(18) 21322

Y Wei et al.

Spectroscopic studies of fuel recycling and impurity behaviors in the divertor region of Wendelstein 7-X

Preprint of Paper to be submitted for publication in
Plasma Science and Technology

This work has been carried out within the framework of the EUROfusion Consortium and has received funding from the Euratom research and training programme 2014-2018 under grant agreement No 633053. The views and opinions expressed herein do not necessarily reflect those of the European Commission.

Spectroscopic studies of fuel recycling and impurity behaviors in the divertor region of Wendelstein 7-X

Y. Wei,[1,2,a] E. Wang,[2] Y. Liang,[2] S. Brezinsek,[2] M. Krychowiak,[3] O. Neubauer,[2] R. König,[3] S. Sereda,[2] Ch. Linsmeier,[2] and W7-X Team[3, b]

[1]*Southwestern Institute of Physics, PO Box 432, Chengdu, People's Republic of China*

[2]*Forschungszentrum Jülich GmbH, Institut für Energie- und Klimaforschung – Plasmaphysik, Partner of the Trilateral Euregio Cluster (TEC), 52425 Jülich, Germany*

[3]*Max Planck Institute for Plasma Physics, 17491 Greifswald, Germany*

[a]*Author to whom correspondence should be addressed. Electronic mail: y.wei@swip.ac.cn*

[b]*Member of the W7-X Team are listed in Nucl. Fusion **53**. 126001 (2013).*

Abstract:

The first divertor operation phase (OP1.2a) was carried out on Wendelstein 7-X in the second half of 2017. The fuel recycling and impurity behaviors in the divertor region were investigated by employing a newly built UV-VIS-NIR overview spectroscopy system. The characteristic spectral lines of working gases (hydrogen and helium), intrinsic impurities (carbon, oxygen and iron) and seeded impurities (neon and nitrogen) were identified and analyzed. The H_α (656.3 nm), He I (587.6 nm), C II (514.5 nm) and O I (777.2 nm) emissions were investigated over a wide range of operating conditions. Results show strong influence of magnetic topology on divertor plasma emissions. The emission levels for H_α, He I, C II and O I are reduced in the order of the standard configuration, the high mirror configuration and the high iota configuration. The impurity behaviors under different plasma conditions are analyzed for both hydrogen and helium discharges.

1. Introduction

The study of fuel recycling and impurity behaviors is a long-standing field of fusion plasma research. It's important to avoid impurity accumulation in improved energy confinement regimes in order to maintain stationary plasma condition. Spectroscopy diagnostics are commonly used as impurity monitor, and the database in this field is by far not as large and detailed for stellarators as for tokamaks. Wendelstein 7-X (W7-X) is currently the world's largest stellarator device. Its goal is to demonstrate the stellarator being an option for future fusion power plants [1]. One major question needed to be addressed is the divertor operation at high power. The W7-X stellarator makes use of the magnetic island divertor concept which utilizes magnetic islands intrinsically formed in the edge magnetic field topology induced by external coils. The influence of impurities on island divertor performance in different island magnetic configurations is being studied to find the optimal magnetic edge topologies for future steady-state operation.

W7-X stellarator achieved its first plasma on the 10th of December 2015 [1, 2]. After initial limiter operation, 10 adiabatically cooling graphite divertor units, known as the test divertor units (TDU), were installed [3]. The first divertor operation phase (OP1.2a) was carried out in the second half of 2017. During this campaign, a UV-VIS-NIR spectroscopy system is employed to study the fuel particle recycling and impurity behaviors in the divertor region [4].

In the present article, we summarized the results of a series of spectral measurements in a wide range of operating conditions during OP1.2a. The experimental setup is described in section 2. The experimental results and discussion are presented in section 3. Spectral surveys were carried out for neon and nitrogen seeded plasmas. The fuel and impurity emissions in different magnetic configurations are studied. And the impurity behaviors under different plasma conditions are analyzed. Summary can be found in section 4.

2. Experimental Setup

The magnetic field configuration of W7-X is entirely generated by 70 external superconducting coils [5], and large magnetic islands are naturally present in the edge. Among the 70 external coils, 50 non-planar coils form the toroidal and poloidal components of the main magnetic field, and 20 planar coils produce the vertical and toroidal components to vary the plasma shape. The rotational transform values (ι) for each magnetic configuration depends on the current settings of the planar coils. Three major divertor configurations with edge iota values (ι_a) of 5/6, 5/5 and 5/4 have been chosen [6]. The mirror ratio for each magnetic configuration is controlled by the current settings of the non-planar coils, and also effects the island positions. The predefined magnetic configurations include the standard configuration, the high iota configuration, the low iota configuration, the high mirror configuration, the low mirror configuration and their derivatives. The test divertor units are placed near the pre-calculated island O-points to open the closed field lines. During OP1.2a, the helium discharges were performed in between the hydrogen discharges as a wall conditioning method and also for commissioning operation scenarios. The plasmas were maintained solely by electron cyclotron resonance heating (ECRH). The heating power for discharges in this study was between 1-6 MW. The line-integrated electron density was in the range of 1-9.1×10^{19} m^{-2} for the helium discharges and 1-3.2×10^{19} m^{-2} for the hydrogen discharges.

A compact overview spectroscopy system was installed on port AEI51 to monitor the fuel and impurity emissions in the divertor region [4]. It views the divertor plasma through a gap between the vertical divertor and horizontal divertor targets. The field of view (FOV) is 10 cm in the horizontal direction and 20 cm in the toroidal direction. The light from divertor plasmas is collected by 800 μm core diameter optical fibers and then transferred to the spectroscopy room outside the torus hall. The overview spectrometer is a combined device with 5 small miniature spectrometers. Each miniature spectrometer has a single input port with a standard SMA905 fiber adapter and different grating settings to cover a certain wavelength range. Together five channels can cover from 300 nm to 1100 nm and provide

simultaneous measurements for hydrogen, helium, carbon, oxygen and other line emissions falling into this wavelength range.

3. Experimental results and discussion

3.1. Spectral survey

A spectral survey was completed with the absolute intensity calibrated overview spectroscopy system. Several characteristic spectral lines of hydrogen and helium were identified. The existing of carbon, oxygen and iron impurities in the plasmas due to plasma-wall interaction was also confirmed by their characteristic spectral lines. Impurity seeding events with neon or nitrogen for radiative cooling were well captured.

Figure 1 shows the overview of a typical hydrogen discharge with neon seeding through the divertor gas inlet [7, 8]. The discharge was performed in reversed field standard configuration. 2.7 MW ECRH power was applied and the core electron temperature was maintained around 4.2 keV. The line-integrated electron density is shown in figure 1(b). The main gas valves were used for H_2 gas fueling, and the divertor gas inlet was used for neon seeding from 3 s to 3.4 s. Figure 1(g-h) shows the spectrum before and during the neon seeding. The identified atoms and ions and their characteristic wavelengths are shown in tables 1 and 2. The hydrogen Balmer lines H_α and H_β were observed. The H_γ and H_δ were usually very weak and overshadowed by nearby O II lines. The H_γ (434.0 nm) was partially overlapped with the OII lines (434.7 nm and 434.9 nm), and the H_δ (410.2 nm) conjoined with the O II line (409.7 nm). The H_α line (656.3 nm) was chosen for monitoring the hydrogen fueling and recycling, and its time trace was shown in figure 1(c). Due to switching back and forth between the helium and hydrogen discharges, strong hydrogen emission was seen in the helium discharges, and strong helium emission in the hydrogen discharges as well. In some hydrogen discharges, helium beam was injected in divertor module 30 for diagnostic purpose, which also contributed to the helium emission in divertor module 51 due to transport inside the magnetic island. Multiple He I lines (587.6 nm, 667.8 nm, 706.5 nm, 728.1 nm and 1083.0 nm) and He II (468.6 nm) were identified. The He I line (587.6 nm) was selected to show the time trace of helium emission, as seen in figure 1(d). Carbon, oxygen and iron emissions were seen in every discharges recorded by the spectroscopy during OP1.2a. A series of CI-CIII, O I-II and Fe I lines are observed, indicating the existing of carbon, oxygen and iron impurities in the plasmas. The C II line (514.5 nm) and O I line (777.2 nm) were used to monitor the evolution of the carbon and oxygen emissions, as seen in figure 1(e-f).

Figure 2 shows a typical hydrogen discharge with nitrogen seeding through the divertor gas inlet. The nitrogen seeding happened at 3-3.32 s and 4.5-4.56 s. Figure 2(g-h) shows the identified and labeled spectral lines before and during the nitrogen seeding. The identified nitrogen lines are listed in table 3. N I-N IV lines were identified while only Ne I-Ne II lines were seen in figure 1, despite the two discharges having very similar parameters. This is due to the fact that in the same ionization stage, nitrogen has lower ionization energy compared to neon.

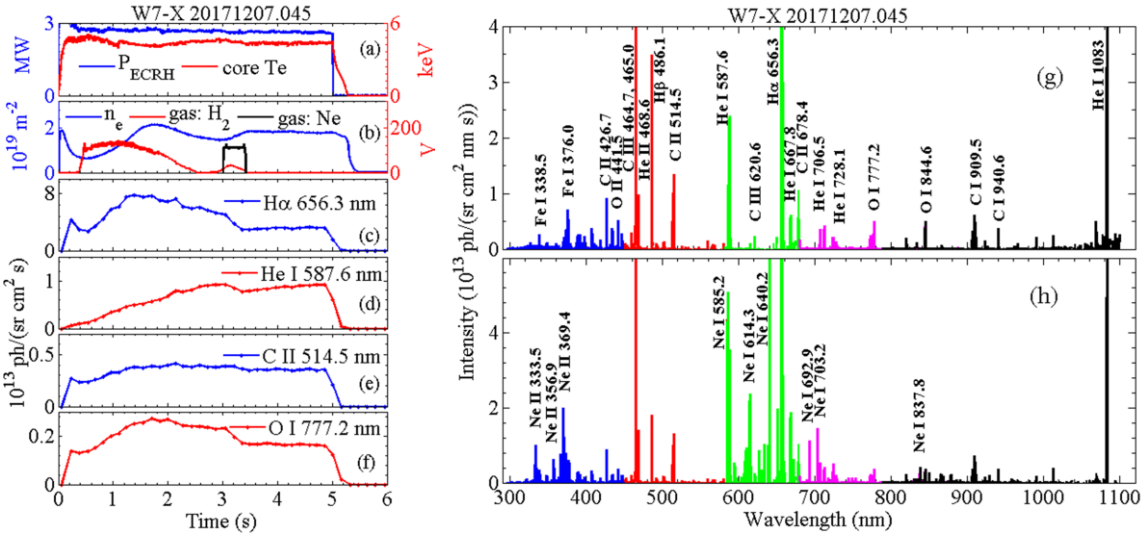

Figure 1. Overview of a typical hydrogen discharge with neon seeding through divertor gas inlet. The time traces in the left figure from top to bottom are (a) the ECRH heating power (P_{ECRH}), and the core electron temperature (core T_e), (b) the line-integrated electron density (n_e), and the valve voltage of main gas fuelling system (H_2) and divertor gas inlet (Ne), (c) the H_α photon flux, (d) the He I photon flux, (e) the C II photon flux and (f) the O I photon flux. The spectrum before and during Neon seeding are plotted in the right figure (g-h) with spectral lines of H, He, C, O, Fe and Ne identified and labeled.

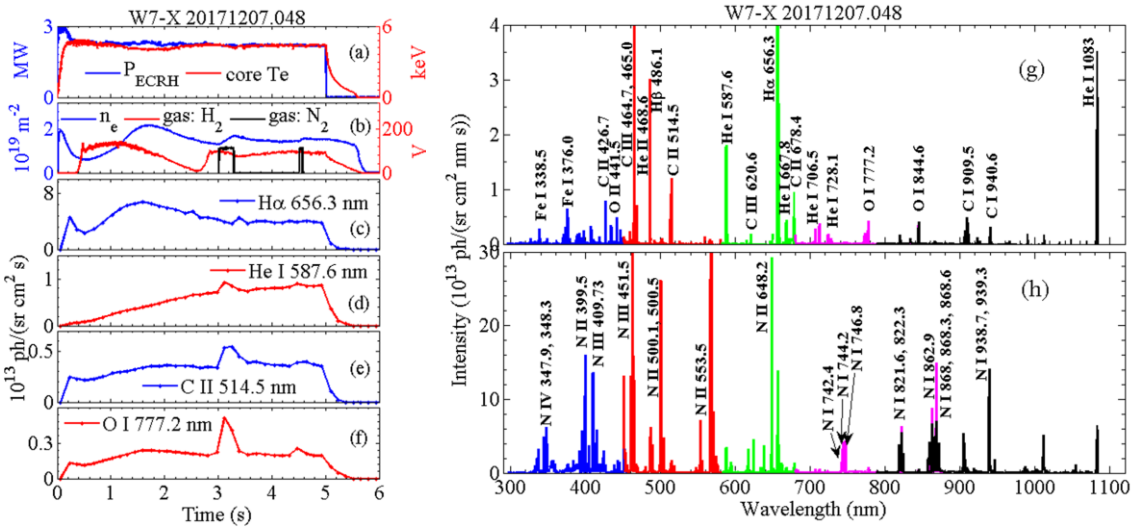

Figure 2. Overview of a typical hydrogen discharge with nitrogen seeding through the divertor gas inlet. The time traces in the left figure from top to bottom are are (a) the ECRH heating power (P_{ECRH}), and the core electron temperature (core T_e), (b) the line-integrated electron density (n_e), and the valve voltage of main gas fuelling system (H_2) and divertor gas inlet (N_2), (c) the H_α photon flux, (d) the He I photon flux, (e) the C II photon flux and (f) the O I photon flux. The spectrum before and during nitrogen seeding are plotted in the right figure (g-h) with spectral lines of H, He, C, O, Fe and N identified and labeled.

Table 1. List of identified spectral lines in W7-X plasmas

Type of line	wavelength (nm)
Fe I	338.5, 376.0
C II	426.7
O II	441.5
C III	464.7, 465.0
He II	468.6
H I(Balmer-β)	486.1
C II	514.5
He I	587.6
C III	620.6
H I(Balmer-α)	656.3
He I	667.8
C II	678.4
He I	706.5, 728.1
O I	777.2, 844.6
C I	909.5, 940.6
He I	1083.0

Table 2. List of identified neon lines in W7-X plasmas during neon seeding

Type of line	wavelength (nm)
Ne II	333.5, 356.9, 369.4
Ne I	585.2, 614.3, 640.2, 692.9, 703.2, 837.8

Table 3. List of identified nitrogen lines in W7-X plasmas during nitrogen seeding

Type of line	wavelength (nm)
N IV	347.9, 348.3
N II	399.5
N III	409.7, 451.5
N II	500.1, 500.5, 553.5, 648.2
N I	742.4, 744.2, 746.8, 821.6, 822.3, 862.9, 868.0, 868.3, 868.6, 938.7, 939.3

3.2. Comparison between hydrogen discharges and helium discharges

During op1.2a, Helium discharges were frequently performed in between hydrogen discharges. Figure 3 shows the time traces of the plasma parameters and the divertor spectral emissions in a typical helium discharge. Compared to the typical hydrogen discharges shown in figure 1 and 2, the three discharges have similar heating power and electron density while the helium discharges has much longer pulse length. In hydrogen discharges, the H_α, C II and O I emission were sensitive to the electron density change, while He I emission slowly raised over time. The main helium source in the hydrogen discharges is the helium neutrals dissolved from the first wall. In some cases, for example in the two discharges shown in figure 1 and 2, helium injection was performed at divertor module 30 (M30), which also contributed the helium emission at divertor module 51 (M51). In typical helium discharge shown in figure 3, the H_α emission is strongly depended on the ECRH power. The H_α intensity decreases 35% while the ECRH power drops from 1.8 MW to 1.2 MW.

Investigations over several helium discharges also show that the averaged H_α intensity increases with increasing ECRH power. The He I emission increases strongly with increasing n_e due to the helium gas fuelling, but only slightly decreases with the dropping ECRH power at 5 s. The C II emission in divertor region is sensitive to the change in ECRH power, but shows very litter response to the helium gas fuelling. The O II emission only shows small changes when the ECRH power drops, and shows no dependence on the changing n_e.

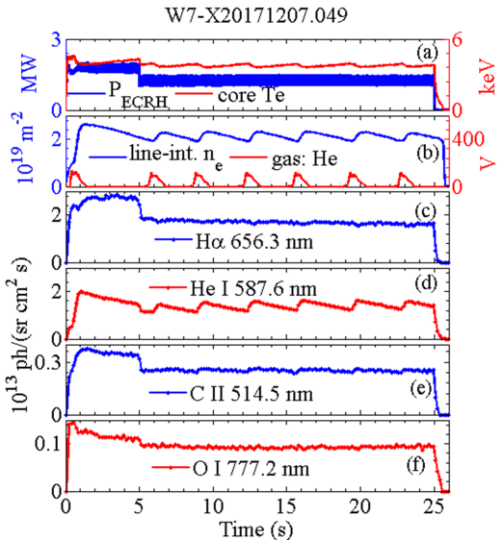

Figure 3. Overview of a typical helium discharge. Time traces of (a) the ECRH heating power (P_{ECRH}) and core electron temperature (core T_e), (b) the line-integrated electron density (n_e) and valve voltage of gas fuelling system (He), (c) the H_α photon flux, (d) the He I photon flux, (e) the C II photon flux and (f) the O I photon flux measured by divertor spectroscopy.

3.3. The influence of magnetic configurations on divertor emissions

During OP1.2a, several magnetic configurations were commissioned. Listed in table 4 are the magnetic configurations which are investigated in this section. The W7-X magnet system can be divided into five identical modules, corresponding to 5 field periods. Due to the periodicity and the stellarator symmetry inside each period, only 5 non-planar coil currents (I1, I2, I3, I4 and I5) and 2 planar coil currents (IA and IB) of half a period are free for variations. By changing the current settings, different magnetic configurations can be achieved. A field line tracing (FLT) code has been applied to trace the field lines with given coil currents [9]. Figure 4 shows the Poincaré plots of the standard configuration, the high mirror configuration and the high iota configuration in the toroidal section of the overview spectrometer. The standard magnetic configuration has a chain of 5 independent magnetic islands naturally present in the plasma edge. The islands are cut open by the horizontal and vertical divertor targets. The viewing geometry of the overview spectrometer is made that in the standard configuration, the island below the upper horizontal divertor is fully covered. The high mirror configuration, as its name suggests, has a higher mirror ratio compared to the standard configuration. In the high mirror configuration, the 5/5 magnetic island chain

Table 4. Magnetic field configuration settings

Configuration	Non-Planar Coil Currents (A)					Planar Coil Currents (A)		Island chain
	I1	I2	I3	I4	I5	IA	IB	
Standard	13068	13068	13068	13068	13068	-700	-700	5/5
High Mirror	13282	13007	12392	11776	11403	-700	-700	5/5
High Iota	14188	14188	14188	14188	14188	-9790	-9790	5/4

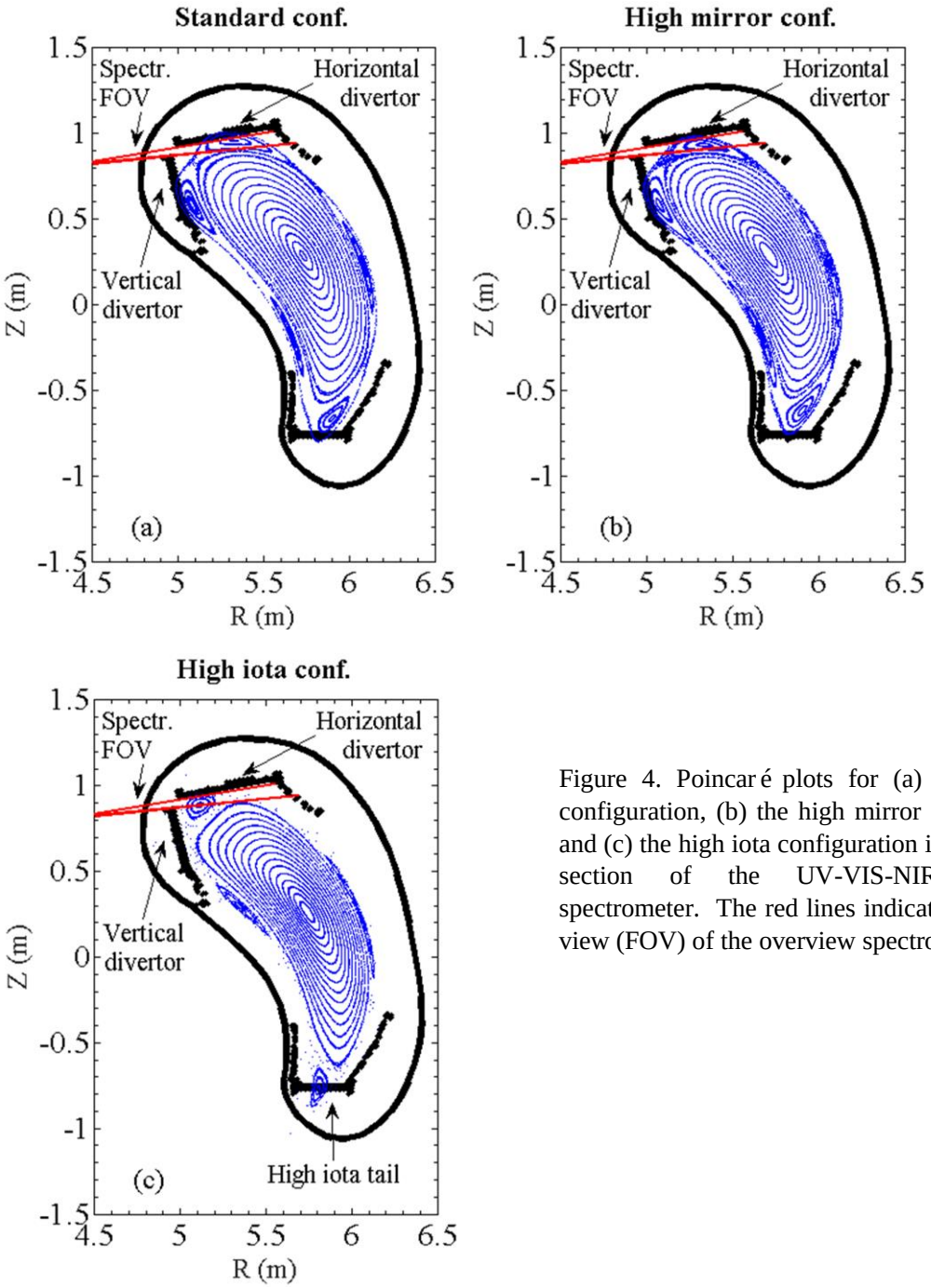

Figure 4. Poincaré plots for (a) the standard configuration, (b) the high mirror configuration and (c) the high iota configuration in the toroidal section of the UV-VIS-NIR overview spectrometer. The red lines indicate the field of view (FOV) of the overview spectrometer.

still present in the plasma edge, but the plasma shape slightly changes. Inside the

spectrometer field of view (FOV), the island position moves downward. In the high iota configuration, a single island is helically winding around the confined plasma region thereby showing up in any poloidal cross section at 4 locations, as seen in figure 4(c). In this configuration, the strike lines are located at the toroidal far end of the top divertor, which for the lower divertor can be seen at the bottom of figure 4(c). This part of divertor target section is commonly referred to as the "high iota tail". In the high iota configuration, there is no strike line anywhere near the location of the FOV of the overview spectrometer.

The spectroscopic measurement shows a strong change of the emission levels in different magnetic configurations. Lower emission levels are seen in the high mirror and the high iota case. In figure 5, comparisons are made among three helium discharges in standard, high mirror and high iota configuration, respectively. As shown in figure 5(a) and (b), these three discharges have similar heating power of around 2.6 MW and electron density of around 3×10^{19} m^{-2}. The H_α (λ = 656.3 nm), He I (λ = 587.6 nm), C II (λ = 514.5 nm) and O I (λ = 777.2 nm) photon fluxes are used to make the comparison between different magnetic configuration, as shown in figure 5(c-f). Going from standard to high mirror, to high iota configuration, the observed intensities of H_α, He I, C II and O I are lower and lower.

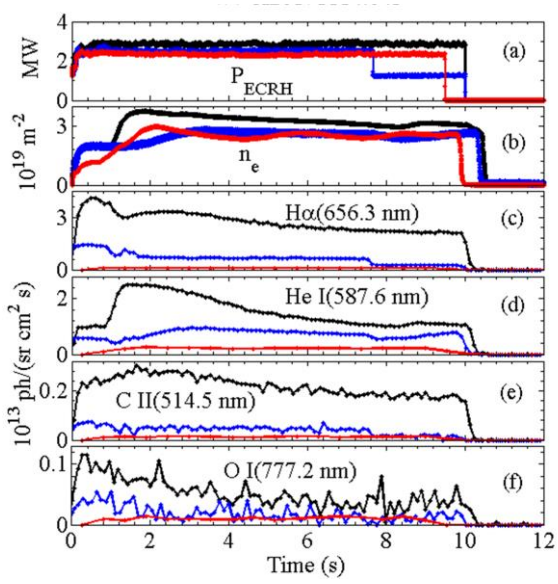

Figure 5. Time traces of (a) the ECRH heating power (P_{ECRH}), (b) the line-integrated electron density (n_e), (c) the H_α photon flux, (d) the He I photon flux, (e) the C II photon flux and (f) the O I photon flux of three helium discharges in the standard configuration (black, W7-X20171114.043), the high mirror configuration (blue, W7-X20171122.011) and the high iota configuration (red, W7-X20171123.016), respectively.

The difference in emission levels could be explained by the different magnetic topology. Figure 6 (a-c) shows the connection lengths of the standard configuration, the high mirror configuration and the high iota configuration at the top divertor region, respectively. The calculation was carried out using the field line tracing tool. The tracing was done both forwards and backwards with an upper limit of 300 m to mark the confined region. All divertor components were considered during the tracing. As shown in figure 6 (a), the view

of the spectrometer covers the whole island near horizontal divertor in the standard configuration. When changing to the high mirror configuration, the confined region of the island reduces significantly, and the field lines near horizontal divertor are partially blocked by components in other toroidal sections. As for the high iota configuration, the strike line move to the high iota tail, this is far away from the observation zone of the overview spectrometer, resulting in the overview spectrometer mainly monitoring the edge scrape-off layer with much shorter connection lengths.

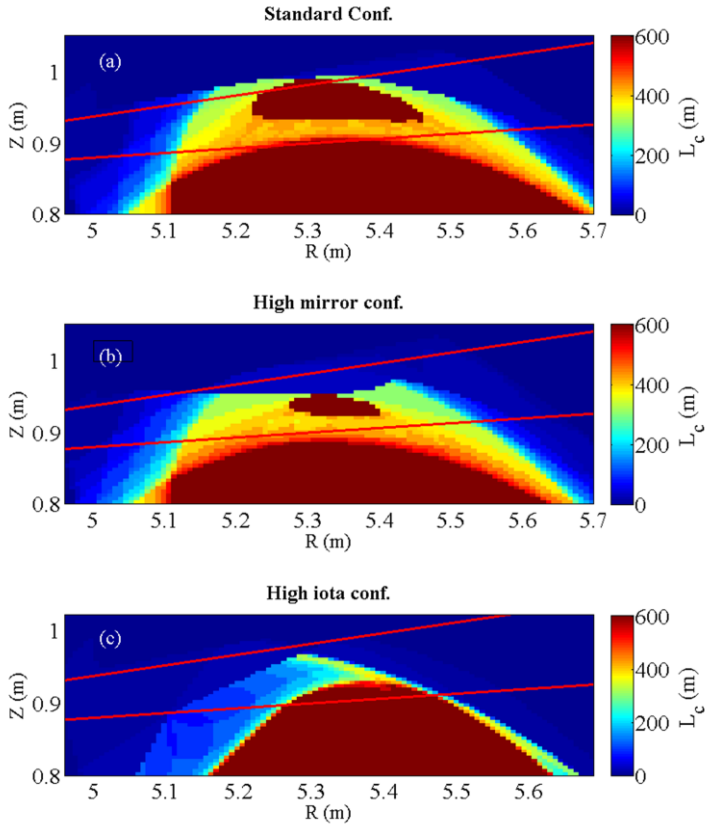

Figure 6. The connection lengths calculated for (a) the standard configuration, (b) the high mirror configuration and (c) the high iota configuration in the upper divertor region. The red lines indicate the FOV of the overview spectrometer.

3.4. Long time evolutions of divertor emissions

In order to study the impurity evolutions, the ionizations per photon (S/XB) were obtained from ADAS [10] with the assumption of an electron temperature of 40 eV and density of 5×10^{18} m^{-3} for the divertor plasmas. By multiplying the S/XB factors with the measured photon fluxes, the particle fluxes can be calculated [11]. Due to the mixture of hydrogen and helium in the plasmas, the sum of hydrogen and helium particle fluxes was employed as normalization factor, and then the particle flux ratios are used to compare between different magnetic configurations.

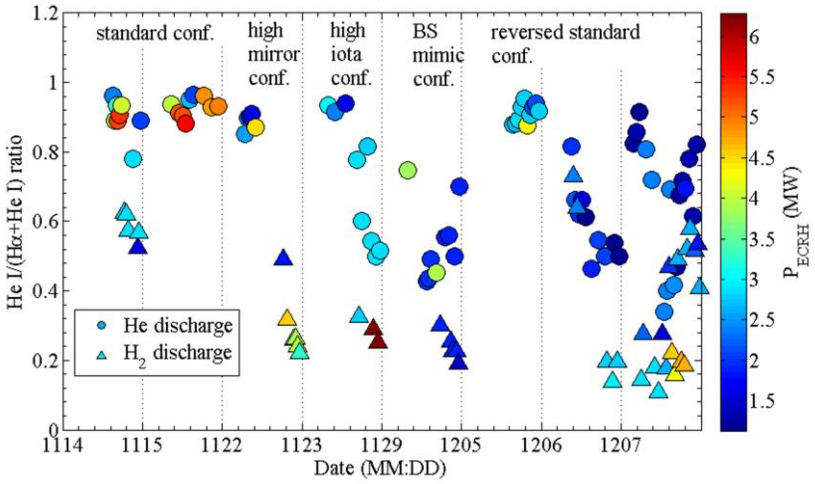

Figure 7. The evolution of particle flux ratio He I/(H_α +He I) in helium and hydrogen discharges as a function of time from November 14th to December 7th .

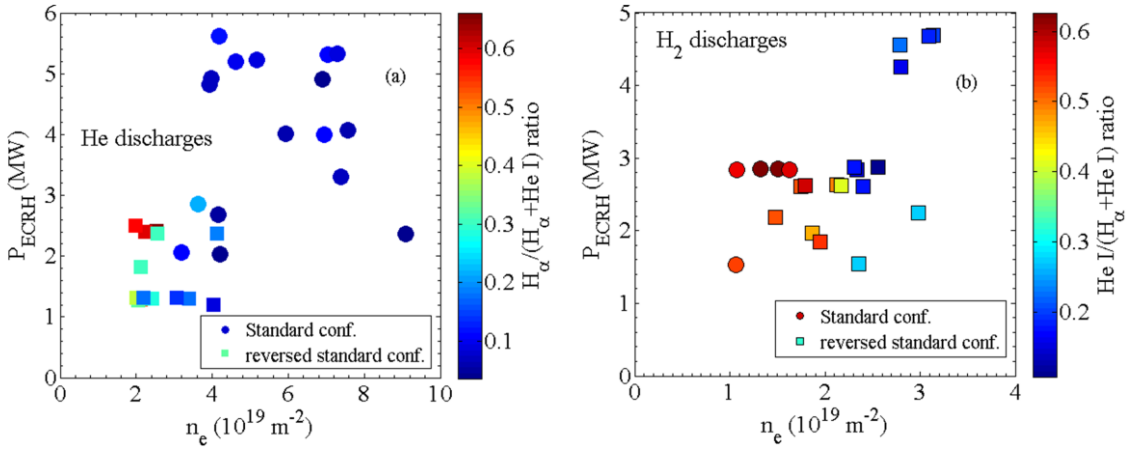

Figure 8. Parametric dependence of the particle flux ratio H_α/(H_α +He I) in helium discharges (a) and the particle flux ratio He I/(H_α +He I) in hydrogen discharges (b) on ECRH heating power and line integrated electron density in standard and reversed standard configuration.

Figure 7 shows the particle flux ratio He I/(H_α +He I) over experimental days for both the hydrogen and the helium discharges. The data cover the experimental days from 14th of November to the 7th of December. During this time period, the magnetic configuration was changed from the standard to high mirror and then to the high iota configuration. On 29th of November, the bootstrap mimic configuration was commissioned to investigate the predicted heat flux overload. On the last experiment week, from 5th to 7th of December, the coil currents were set to reversed direction to investigate any possible up/down asymmetries due to particle drifts between the upper and lower divertors. Due to instrument failure or poor plasma conditions, not all discharges during these experimental days have usable data. Of each available discharge, the spectral data was chosen from a central phase of 1 s in the ECRH power flat-top phase without fueling or impurity seeding. On experimental days which only the helium discharges were performed (e.g. 15th of November and 5th of

December), the He I/(H_α +He I) ratio was above 0.8. The hydrogen release in continuous helium discharges shows no downward trend over discharges, while higher hydrogen concentration can be seen with higher heating power. During the experimental days when hydrogen and helium discharges took the turns (e.g. 14th of November, 23rd of November, 29th of November and 6th of December), frequent helium cleaning discharges caused helium particles trapped in the wall and slowly being released afterwards. A clear decrease of the He I/(H_α +He I) ratios can be seen in helium discharges as well as in hydrogen discharges over those days, especially after a series of hydrogen discharges without helium discharges in between, suggesting the helium can more easily be replaced by hydrogen. On 7th of December, the ECRH heating power varied rapidly within 1.2-4.6 MW, which strongly effected the H_α emission. The helium discharges were performed more frequently, which fueled the helium emission. So the trend of the He I/(H_α+He I) ratios in this day is more scattered than on other days.

Due to the strong effect of the magnetic configurations on divertor topology and emission level, the emission in standard and reversed standard configuration is used to catalog the influence of plasma parameters such as heating power (P_{ECRH}) and electron density (n_e) on hydrogen and helium release. The two configurations have the same coil current values but reversed current direction, resulting in identical magnetic topology. Figure 8(a) shows the H_α/(H_α+He I) ratios in P_{ECRH}-n_e diagram to demonstrate the hydrogen release in helium discharges. For helium discharges in the reversed standard configuration, the available discharges being crowded in the small region of 1-3 MW heating power and 2-4×10^{19} m^{-2} electron density, the hydrogen concentrations increase with increasing heating power and decrease with increasing electron density. For helium discharges in standard configuration, most available discharges are performed under high heating power and high electron density, and the H_α/(H_α+He I) ratios are usually lower than 0.3. For helium release in hydrogen discharges, as shown in figure 8(b), the He I/(H_α+He I) ratios reach 0.6 in the low n_e and high P_{ECRH} region.

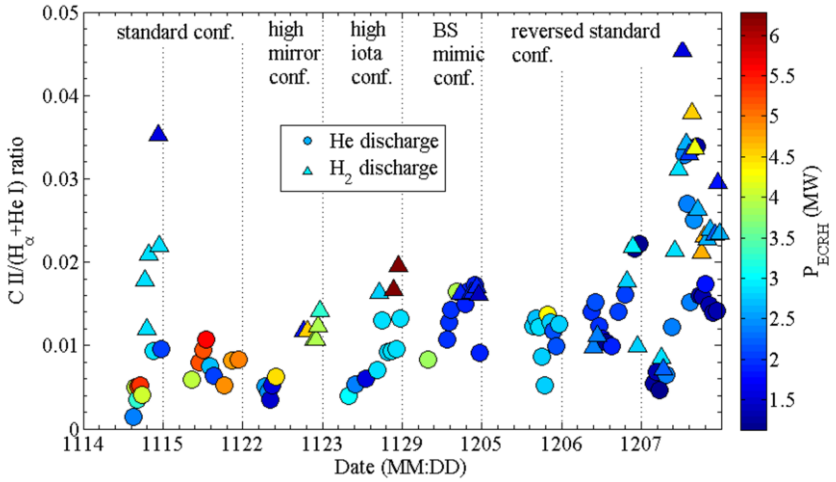

Figure 9. The evolution of particle flux ratio C II/(H_α +He I) in helium and hydrogen discharges as a function of time from November 14th to December 7th .

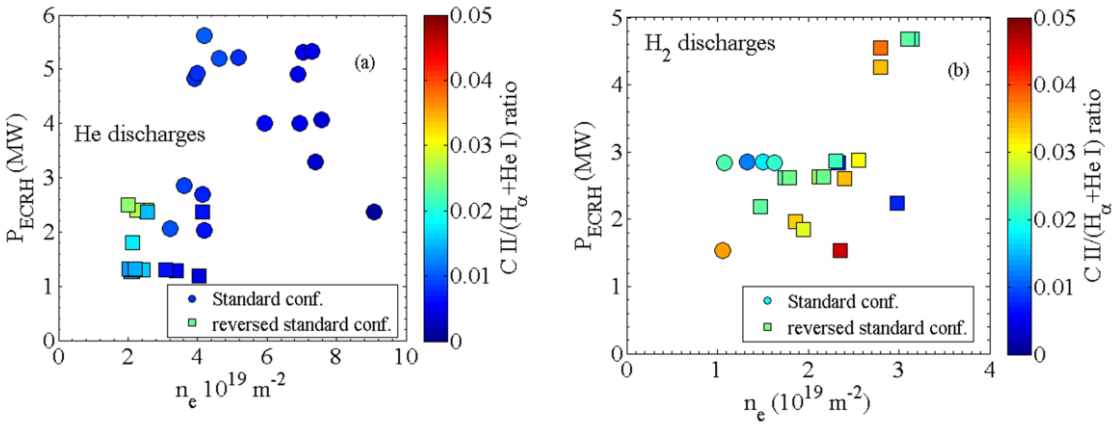

Figure 10. Parametric dependence of particle flux ratio C II/(H_α +He I) in helium discharges (a) and in hydrogen discharges (b) on ECRH heating power and line integrated electron density in standard and reversed standard configuration.

The carbon emission in the divertor region has been studied using low ionization stage spectral lines of carbon such as C II line (λ = 514.5 nm). Figure 9 shows the long time evolution of the normalized carbon intensities C II/(H_α+He I) in helium and in hydrogen discharges. Clearly lower levels of Carbon emission are seen in high mirror and high iota configuration. This is consistent with the connection length calculation in section 3.2, which show that there are little to no sources near the FOV, therefor only very small carbon fluxes and then only low C II emission can be expected. Figure 10 shows the C II/(H_α+He I) ratios in the the P_{ECRH}-n_e diagram. In helium discharges, the C II/(H_α+He I) ratios remains low in the standard configuration, While the C II/(H_α+He I) ratios in the reversed standard configuration falls in the low n_e region and the ratios increase with increasing ECRH power, and decrease with decreasing n_e, as seen in figure 10(a). In hydrogen discharges, as shown in figure 10(b), the normalized carbon emission shows no clear dependence on ECRH power or electron density.

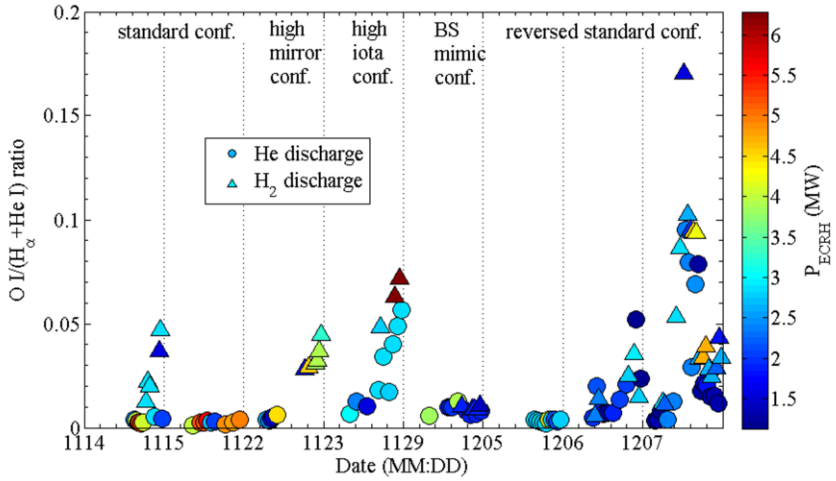

Figure 11. The evolution of particle flux ratio O I/(H_α +He I) influx ratios in helium and hydrogen discharges as a function of time from November 14th to December 7th .

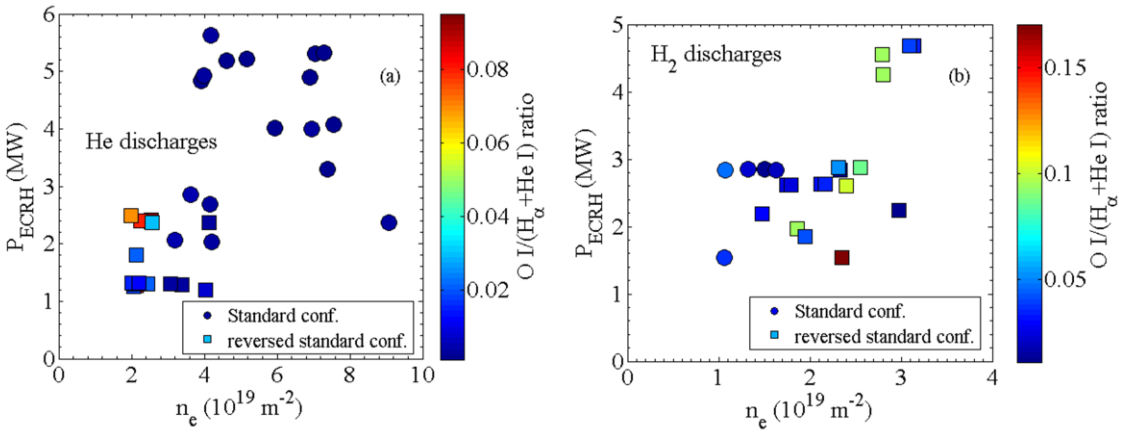

Figure 12. Parametric dependence of particle flux ratio O I/(H_α +He I) in helium discharges (a) and in hydrogen discharges (b) on ECRH heating power and line integrated electron density in standard and reversed standard configuration.

Strong oxygen emission was seen through the whole experiment campaign. The main suspects are the oxygen introduced into vessel by newly installed divertor components. As shown in figure 11, for experimental days on which only helium discharges were performed (e.g. 15th of November and 5th of December), the O I/(H_α +He I) ratios are below 0.01. On 14th and 22nd of November, although the O I/(H_α +He I) ratios remain low in the helium discharges, a clear increase of O I/(H_α +He I) ratios is seen in the hydrogen discharges. On the 23rd of November, the 6th and 7th of December, the O I/(H_α +He I) ratios raises significantly over time. The change of heating power and electron density has very litter influence on the oxygen emission level, as seen in figure 12. Since the main oxygen sources are the newly installed divertor components, and the increase of oxygen emission shows strong time dependence, once can guess it may due to the surface temperature raise. During the experimental day, the test divertor units relied on the inertial cooling. The several minutes break between discharges allowed the surface to cool down to a safety level for the next discharge, but still the heat accumulated on the divertor surface, causing more oxygen release from the panel.

4. Summary

The fuel recycling and impurity behaviors in the divertor region during the W7-X first divertor operation phase (OP1.2a) has been investigated by the using the divertor spectroscopy data. The spectral lines of the working gas hydrogen and helium, as well as the intrinsic impurities carbon, oxygen and iron were identified. Multiple neon and nitrogen lines were also identified during impurity seeding. The H_α (656.3 nm), He I (587.6 nm), C II (514.5 nm) and O I (777.2 nm) line emissions are investigated over a wide range of operating conditions. Results show the magnetic topology significantly affects the divertor emission level. The emission levels for H_α, He I, C II and O I decrease in the order of the standard configuration, the high mirror configuration and the high iota configuration, corresponding to the shrinkage of connection length, which resulting in a lack of sources

near or inside the view of the divertor spectroscopy. The evolution of the He I/(H_α +He I) ratios over experimental days shows that the plasmas are actually a mixture of hydrogen and helium due to the strong recycling from wall. The survey in standard and reversed standard configuration shows that the hydrogen removed from the wall by helium discharges is most efficient with low plasma electron density and high ECRH power, while the carbon yield is also enhanced. Outgassing of water from hot targets causes strong O I emission in the divertor region. Further wall conditioning such as boronisation is necessary for reducing the oxygen influxes.

Acknowledgments

This work has been carried out within the framework of the EUROfusion Consortium and has received funding from the Euratom research and training programme 2014-2018 under grant agreement No 633053. The views and opinions expressed herein do not necessarily reflect those of the European Commission. The authors are thankful for the support from the China Scholarship Council. This work is also supported by the National Natural Science Foundation of China under Grant No. 11675050.

References

[1] R C Wolf *et al* 2016 IEEE Transactions on Plasma Science 44(9) 1466
[2] T Klinger *et al* 2017 Plasma Phys. Control. Fusion 59 014018
[3] A. Peacock *et al*. 2009 Fusion Engineering and Design 84 1475–1478
[4] Y. Wei *et. al.* 2018 AIP Advances 8 085011
[5] T Rummel *et al* 2012 IEEE Transactions on Plasma Science, 40(3), 769
[6] Y Feng 2013 Journal of Nuclear Materials 438, S497
[7] Barbui *et al* 2016 Rev. Sci. Instrum. 87 11E554
[8] Krychowiak *et al* 2016 Rev. Sci. Instrum. 87 11E554D304
[9] S Bozhenkov et al 2013 Fusion Eng. Des. 88 2997–3006
[10] http://www.adas.ac.uk/adaseu.php
[11] S Menmuir et al 2006 Phys. Scr. 74 439-448